International Journal of Computational and Theoretical Chemistry
2026, Vol. 14, No. 2, pp. 34–48
https://doi.org/10.11648/j.ijctc.20261402.11

SciencePG
Science Publishing Group

Research Article

Theoretical Approach of the Rational Design of Methoxy Diphenylamine-Substituted Fluorine-Based HTMs for Highly Efficient Perovskite Solar Cells: DFT/TD-DFT

Abaid Ullah[1], Usman Ibrahim[1], Samina Liaqat[2], Muhammad Javid[1,*], Wajiha Shehbaz[3], Rimsha Shareef[1], Sabahat Asghar[3], Muhammad Sajid Abbas[4], Muhammad Hasnain[1]

[1]Department of Chemistry, University of Agriculture, Faisalabad, Pakistan

[2]Department of Chemistry, Government College University Faisalabad, Pakistan

[3]Institute of Chemistry, Khwaja Fareed University of Engineering and Information Technology, Rahim Yar Khan, Pakistan

[4]Department of Physics, University of Agriculture, Faisalabad, Pakistan

Abstract

Organic solar cells (OSCs) have attracted significant attention as a promising photovoltaic technology because of their low fabrication cost, lightweight nature, mechanical flexibility, and rapid improvement in power conversion efficiency (PCE). Despite these advances, the development of efficient hole-transporting materials (HTMs) remains a major challenge for further enhancing device performance. In this study, density functional theory (DFT) and time-dependent density functional theory (TD-DFT) calculations were employed to rationally design and investigate a series of four methoxy-substituted diphenylamine-based fluorine-containing hole-transporting materials (MDFM1–MDFM4) for photovoltaic applications. The molecular structures were engineered by functionalizing a fluorine-based core with methoxy diphenylamine donor units and terminal acceptor groups, connected via thiophene π-bridges, to improve their optoelectronic properties. The designed molecules were systematically evaluated for frontier molecular orbital energies, energy band gaps, reorganization energies, absorption spectra, charge-transfer characteristics, and photovoltaic parameters. The computational results reveal that structural modification significantly influences the electronic and optical properties of the investigated HTMs. Among the designed compounds, MDFM4 exhibits the most promising performance, with the smallest HOMO–LUMO energy gap (4.44 eV), the lowest electron reorganization energy (0.0144 eV), and the longest maximum absorption wavelength (455 nm in the gas phase), indicating enhanced charge transport and broader light-harvesting capability. In addition, MDFM4 demonstrates improved photovoltaic characteristics, including a higher predicted open-circuit voltage and superior overall photovoltaic performance compared with the reference molecule. These findings demonstrate that rational molecular engineering through terminal acceptor modification is an effective strategy for tuning the optoelectronic properties of fluorine-based HTMs. The present theoretical investigation provides valuable insights for the future design and development of high-performance hole-transporting materials for next-generation organic solar cells.

*Correspondence: Muhammad Javid (javidkhanchemist@gmail.com)

Received: 3 July 2026; **Accepted:** 20 July 2026; **Published:** 10 August 2026

Keywords

Photovoltaic, Quantum, Optoelectronic Properties, Methoxy Diphenylamine, Thiophene

1. Introduction

Renewable energy sources have become a more attractive and attention-gaining topic nowadays [1]. Though future energy shortages are possible, they may be avoided with the help of renewable energy sources like solar, wind, fuel cells, and biomass [2]. Sunlight is a primary source of energy that can be used across the globe [3]. The main challenge was to transform light into electricity efficiently, optimizing the utilization of this abundant energy resource [4]. Multiple kinds of photovoltaic device components were made that can change sunlight into electrical power [5]. However, these photovoltaic devices are too costly. Silicon has been utilized extensively in photovoltaic cells because of its numerous advantages, including its non-toxic nature, high- efficiency power conversion (PCE), reliability, and accessibility [6]. On the other hand, recently, a marked reeducation in the utilization of silicon has been seen due to its stable energy states, embrittlement, and high expenditure [7].

The organic photovoltaic cell, also known as the third-generation solar cell, is a revolutionary device that harvests solar light more efficiently than second-generation solar cells, converting it into electricity [8]. Donor and acceptor molecules exhibit numerous ideal properties that is, such as optoelectronic, chemical, and structural properties) to determine the performance of OSCs [9]. In organic photovoltaics (OPVs), a heterojunction is predominantly established between donor and acceptor materials [10]. The maximum power conversion efficiency (PCE) achieved in the previous reported studies for OSCs is 19.9% [11].

In the recent decade, fluorine and its derivatives have become more favorable in specific electron mobility and greater electron affinity that can be used as an ETL in OSCs [12]. The PCE of fluorine-based devices cannot be achieved by more than 18% due to high purification requirements, and absorption is inherent in the visible and near-infrared regions [13]. The fabrication process is cost-effective, and the requirements of high purity have controlled the utilization of fluorine in OPVs [14]. Remarkable optoelectronic features and higher molar absorption coefficient in visible regions have made the non-fluorine-based small molecule promising candidates that can be used as electron acceptor materials [15]. In NF acceptors, the charge mobility can be improved by integrating the electrophilic species [16]. Moreover, their preference for edge-to-face π-stacking interactions, attributed to the spatial arrangement of methoxy groups and aromatic rings within the molecule, suggests potential benefits in charge transport and overall device performance [17]. These distinctive qualities, methoxy diphenylamine derivatives, offer the prospect of contributing to the advancement of organic solar cell technology (OSCT) [18].

Here, we designed four hole-transporting materials (HTMs) using fluorine as a base, namely MDFM1, MDFM2, MDFM3, and MDFM4. These materials were developed by incorporating terminal acceptors through a thiophene-based bridge [19]. The inclusion of thiophene, acting as a pi-bridge, was chosen because of its advantageous optoelectronic features and impressive hole mobility [19]. This makes it particularly appealing for the production of HTM in organic photovoltaic cells (OPVs) [20]. The terminal acceptors, specifically cyano, thiazolidine, methoxy, and pyridine, were strategically employed to modify the molecular energy levels [21]. This modification aimed to assess the photovoltaic capabilities of the specially designed HTMs [22]. The results of this investigation demonstrated that all the HTMs created (MDFM1, MDFM2, MDFM3, and MDFM4) exhibit potential for use in environmentally friendly, high-efficiency organic solar cell fabrication.

2. Computational Details

The density functional theory has been given vast emphasis in the theoretical area to determine the charge conductance, geometry, and photophysical and electric properties of the under study molecules, also their good results are linked to the basis sets applied in the calculations. All computational calculations are carried out through Gaussian 09 software. Various basis sets have different parameters in the calculations, such as ionization potentials (IP), electron affinity (EA), hole/electron-transporting strength, molecular orbitals (MO), etc. The B3LYP is considered a size usually applied for mid-sized organic molecules. The benchmarking method was evaluated for the choice of the functional and basis set. The four functionals, including B3LYP, CAM-B3LYP, MPW-1PW91, and WB97XD, were used in the gaseous and solvent (DCM) phases with a 6-31 G (d, p) basis set using the solvation model, the Integrated Equation Formalism Polarizable Continuum Model (IEFPCM). The computations were conducted utilizing 6-31G (d, p) models. To find out the most suitable functional for calculation, we performed calculations on B3LYP, CAM-B3LYP, MPW1PW91, ωB97XD, and the results were 513.6nm, 422.4nm, 488nm, and 305.07nm, respectively, in the UV/visible spectrum. We used the CAM-B3LYP method

for further investigation, because the calculated value of the reference MDF (422.4nm) in the reported experimental calculation closely corresponds to the calculated values through the use of CAM-B3LYP and 6-31G (d, p) model. Therefore, the molecular geometries have been universally optimized with B3LYP/ 6-31 G (d, p) to determine the equilibrium molecular structures. Subsequent required analyses were accomplished with the identical DFT level of theory. The predicated the diabatic IE and adiabatic IP were applied to determine the absolute chemical hardness by Koopman's theorem. The Charge transfer (CT), chemical softness, and hole/electron mobility are also analyzed. PDOS analysis has been performed using PyMOlyze 6.2 software to evaluate the effect of molecular orbital contributions. However, the UV–vis highest absorption spectrum of the designed molecules has been optimized using the TD-DFT level of theory for the ten excited states of the molecules. The UV–Vis spectrum and transition density matrix (TDM) were visualized with Multiwfn 3.5. The reorganization energy (RE) is an efficient determinant of charge mobility carriers. Consequently, the total RE could be composed of an external RE that came from the external solvent organic molecules and internal RE derived from the reactant molecules, and is calculated as the addition of RE_{hole} and $RE_{electron}$ energy values. Based on the optimized neutral, cationic, and anionic structures, the RE for the hole and electron of the organic molecules were predicted from the single-point energy calculations. RE for hole and electron can be calculated using the Equations (1) & (2).

$$RE_{hole} = [E_+^0 - E_0] + [E_0^+ - E_+] \quad (1)$$

$$RE_{electron} = [E_-^0 - E_0] + [E_0^- - E_-] \quad (2)$$

The hole (λh) and electron (λe) reorganization energies were calculated using Equations (1) and (2), respectively. In these equations, (E_0) represents the total energy of the neutral molecule at its optimized ground-state geometry. (E_+^0) is the energy of the cation calculated at the optimized geometry of the neutral molecule, while (E_+) denotes the total energy of the optimized cationic species. Similarly, (E_-^0) is the energy of the anion calculated at the optimized geometry of the neutral molecule, whereas (E_-) is the total energy of the optimized anionic species. The terms (E_0^+ and (E_0^-) represent the energies of the neutral molecule evaluated at the optimized geometries of the cation and anion, respectively.

All quantum chemical calculations were performed in tetrahydrofuran (THF) using the Integral Equation Formalism Polarizable Continuum Model (IEFPCM) at the CAM-B3LYP/6-31G(d,p) level of theory. The UV–Vis absorption spectra were generated using OriginPro software. The charge-transport properties of the reference molecule (MDF) and the designed molecules (MDFM1–MDFM4) were evaluated based on their hole (λh) and electron (λe) reorganization energies. Lower reorganization energy values indicate reduced structural relaxation during charge transfer, leading to higher charge-carrier mobility and improved charge-transport performance. Therefore, the calculated reorganization energies provide an important criterion for assessing the suitability of the designed molecules as efficient hole-transporting materials for organic solar cell applications.

3. Results and Interpretations

3.1. Optimized Structures

A reference molecule, MDF and design molecules (MDFM1-MDFM4) have been optimized under the functional Coulomb-Attenuated-Method-B3LYP utilizing the 6-31G (d, p) basis set model [23]. Determining the parameters of the optimized structures and molecular geometries transformation from the ground state to the oxidized structural state is important for identifying the charge mobility and geometrical stabilization of organic molecules [24]. To understand the shape properties of the under-studied molecules, ground-state geometries were optimized using the B3LYP with the 6-311G (d, p) level of method. Notably, structural parameters, such as dihedral angles (θ) and bond lengths (l), have been investigated in the main fragments, such as MDF-based acceptor (A), thiophene-based spacer to accepting units, and spacer to donor (D) fragments. The main objective was to analyze the planarity and geometrical deformations from the ground state to excited state structures, which are necessary for the charge carriers in the molecules. The dihedral and bond distances are shown in Table 1. The optimized geometries are displayed in Figure 1.

The bond lengths between the acceptor and donor fragments, where the spacer is absent are 1.9053 Å, 1.9069 Å, 1.9082 Å, and 1.9180 Å. At the same time, 1.092 Å is the reference molecule MDF, and the bond distances between acceptor, spacer, and donor units are 1.4598 Å, 1.4814 Å, and 1.4621 Å length recorded between the donor and spacer fragments, and 1.6951 Å, 1.8378 Å, 1.6358 Å between the spacer and acceptor fragments. All the designed molecules have much more important bond lengths, increasing flexibility and the steric effect. The dihedral angles efficiently evaluate geometrical properties such as orientation, planarity, steric effect, and flexibility, which affect intermolecular charge transmission. In molecules MDFM1-MDFM4, the donor-acceptor angle in MDFM1, MDFM2, MDFM3, and MDFM4 ranges from 15.4167° to 57.1953° without adding the spacer. The dihedral angle between Si- based donor and spacer fragments shows 3.8174° to 7.8938° degrees, whereas the spacer and acceptor range from 1.49° to 6.12° degrees.

Table 1. *Bond distance (d_1) between donating segments and acceptance segments, donor and bridge, the bond distance (d_2) between bridging part and accepting part, the bond angle between donor and spacer (θ_2), and between spacer and acceptor (θ_2).*

Molecules	Bond length (d_1)	Bond Length (d_2)	Bond angle (θ_1)	Band angle (θ_2)
MDF	1.092	---	0.0692	---
MDFM1	1.9053	1.4598	3.4829	---
MDFM2	1.9069	1.4814	19.4167	3.8174
MDFM3	1.9082	---	57.1953	---
MDFM4	1.9180	1.4621	7.2541	7.8938

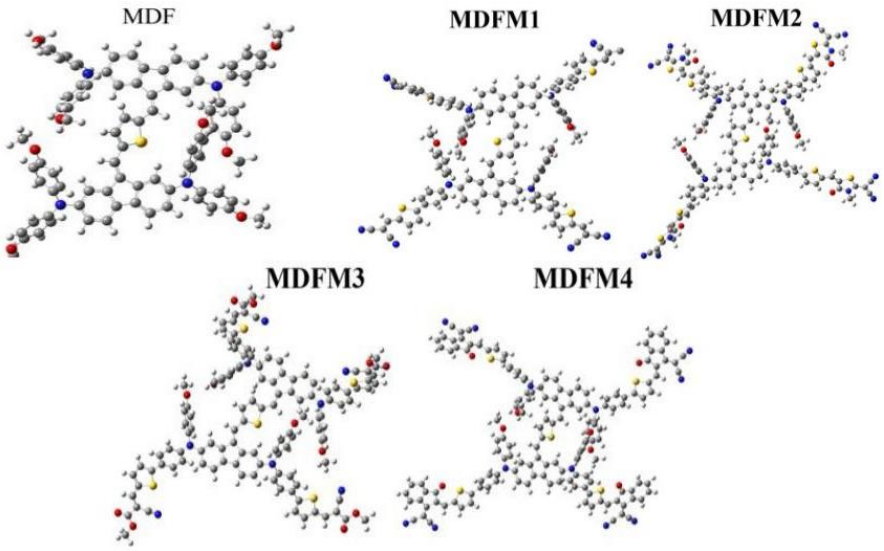

Figure 1. *At the CAM-B3LYP as well as 6-31G (d, p) theory level, optimized MDF's molecular structures and developed molecules (MDFM1-MDFM4).*

3.2. Frontier Molecular Orbitals

The utilization of frontier molecular orbitals (FMOs) in organic solar cells has led to a better understanding of their excited state properties, aiding advancements in the charge transmission process [25]. This progress has contributed to enhanced charge transmission mechanisms for higher photovoltaic efficiency in small molecule-based organic photovoltaic cells [26]. Optimizing electron transfer and energy levels can increase solar cell efficiency. HUMO and LUMO distributions can impact performance and conversion processes.

Table 2. *Representative molecule MDF and MDFM1-MDFM4's bandgap energy, EHOMO, and ELUMO values.*

Molecule	EHOMO (eV)	ELUMO (eV)	Eg (eV)
MDF	-5.472	-1.029	4.443
MDFM1	-6.320	-1.911	4.409
MDFM2	-6.269	-1.967	4.302
MDFM3	-6.036	-1.519	4.517
MDFM4	-6.148	-2.152	3.996

The estimated HOMO-LUMO bandgap Eg values are utilized as an energy differential between the levels and a stability index. The rise in conductance is linked to the drop in energy gap (Eg).

The E_{H-L} and E_g energies are shown in Table 1. The figures of E_{HOMO} of reference molecule MDF are -5.47 eV, whereas the E_{LUMO} value is -1.03 related to the HOMO- LUMO band gap of 4.44 electron Volts. The E_{HOMO} and E_{LUMO} values of MDFM1, MDFM2, MDFM3, and MDFM4 were obtained using the CAM-B3LYP technique with the 6-31G model of DFT in Figure 3. The computed E_{HOMO} values were -6.320 eV, -6.269 eV, -6.036 eV, and -6.148 eV, respectively, whereas the ELUMO values were -1.911 eV, -1.967 eV, -1.519 eV, and 2.152 electron volts. Reference MDF and developed molecules (MDFM1-MDFM4) have HOMO and LUMO band gaps of 4.443 eV, 4.409 electron volts, 4.302 eV, 4.517 electron volts, and 3.996 electron volts, respectively. Among developed molecules, MDFM1 showed the low value difference with the reference molecule, which indicates that it is more stable than the other designed compounds. In comparison to a representative compound, all design compounds have a lower EH-L, which allows all designed molecules to reveal charge transfer processes more readily. MDFM4 has a significant charge transfer mechanism since its energy gap value (4.00 eV) is smaller than that of any other developed molecules. The substances MDFM1, MDFM2, MDFM3, and MDFM4 are designed with significantly lower HOMO values, which can potentially enhance the open circuit voltage (Voc) of devices utilizing OSCs.

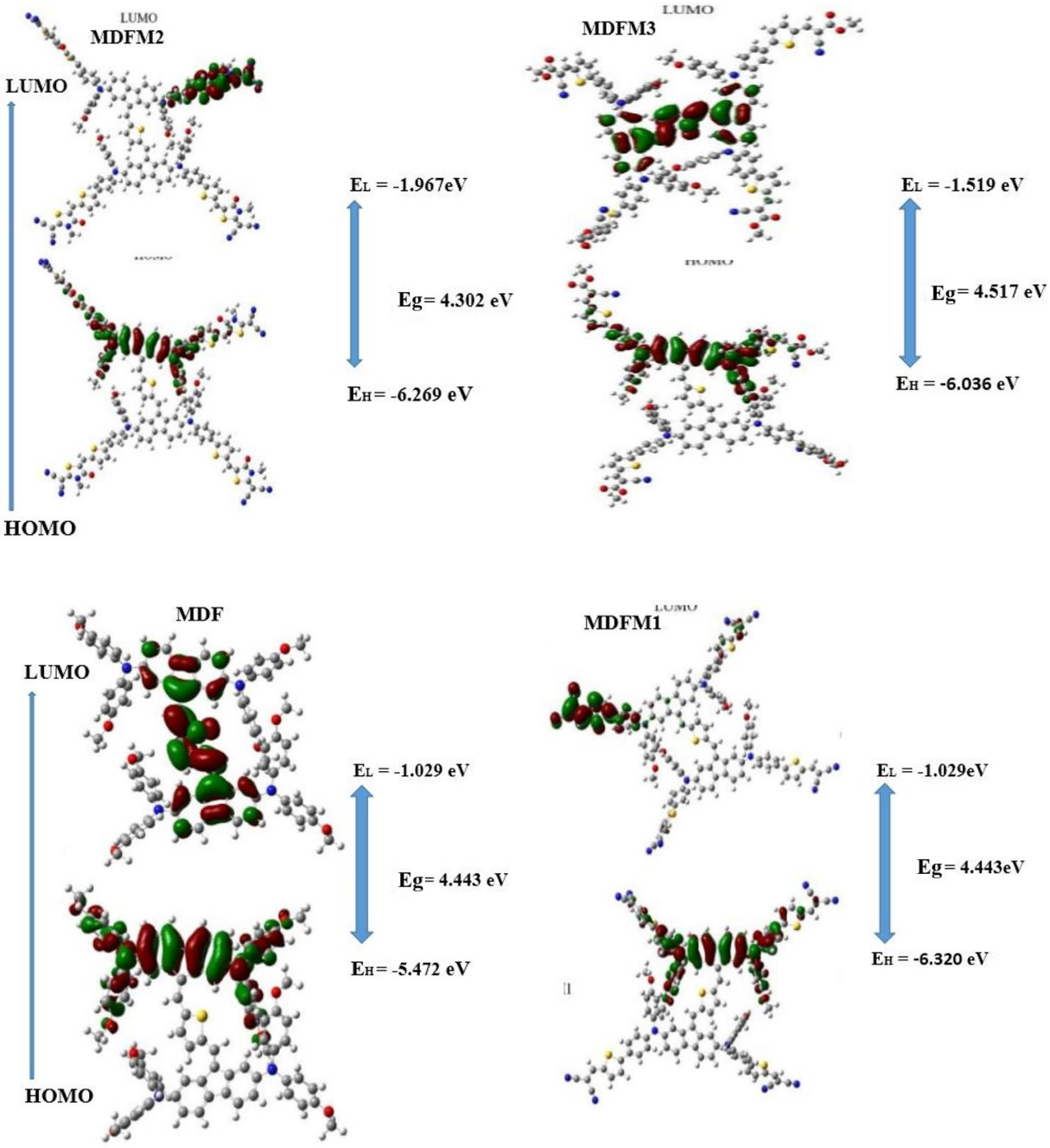

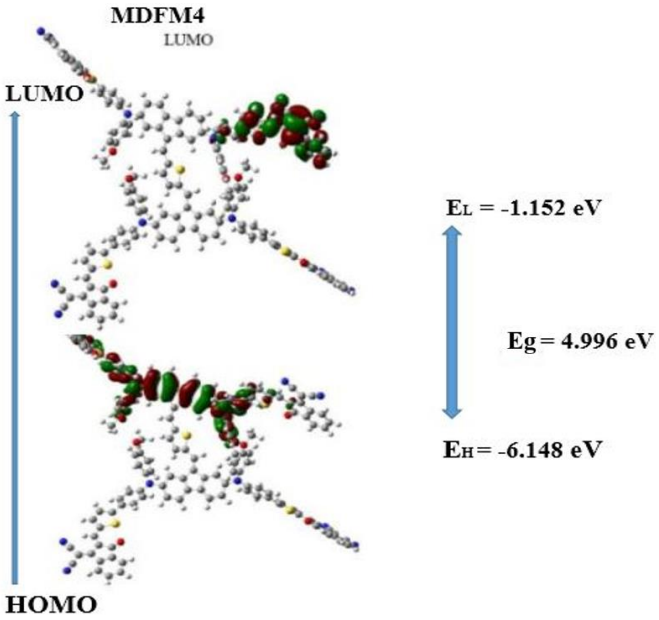

Figure 2. *FMO diagrams of representative MDF developed molecules MDFM1, MDFM2, MDFM3, and MDFM4 at CAM-B3LYP with 6-31G hybrid model.*

3.3. Spectroscopic Analysis

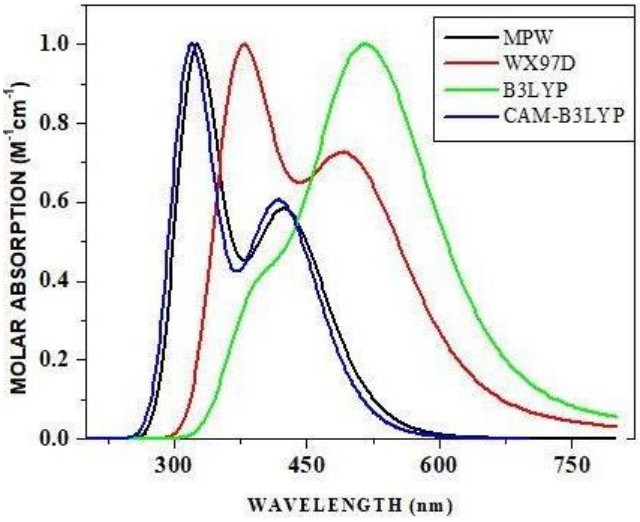

Figure 3. *Shows the wavelength and absorption relationship.*

3.4. Electronic Density of State Analysis

Mulliken charge distribution has been utilized to confirm the FMO (Frontier Molecular Orbital) results [27]. The molecular fragment's impact on the bonding (HOMO) and antibonding (LUMO) molecular orbits has been determined through the use of electronic density of State (EDOS) analysis [28]. Additionally, the PDOS calculations have been used to find out the E_{HOMO} and E_{LUMO} orbitals. The PyMolyze 1.1 program was employed to transform the EDOS modeling, which was calculated using the designated DFT schemes, for MDF and MDFM1-MDFM4. To analyze the DOS, MDF has one part, which is the core, that gets the PDOS graphs. In contrast, the unrestrained MDFM molecules (MDFM1-MDFM4) were split into three small portions-acceptor, bridge, and core-depicted by the colors blue, green, and red, respectively, in the DOS charts displayed in Figure 4. The E_{HOMO} and E_{LUMO} values are indicated by negative and positive values along the x-axis in the PDOS diagrams, respectively, while the energy gap (Eg) is shown by the energy gap between them.

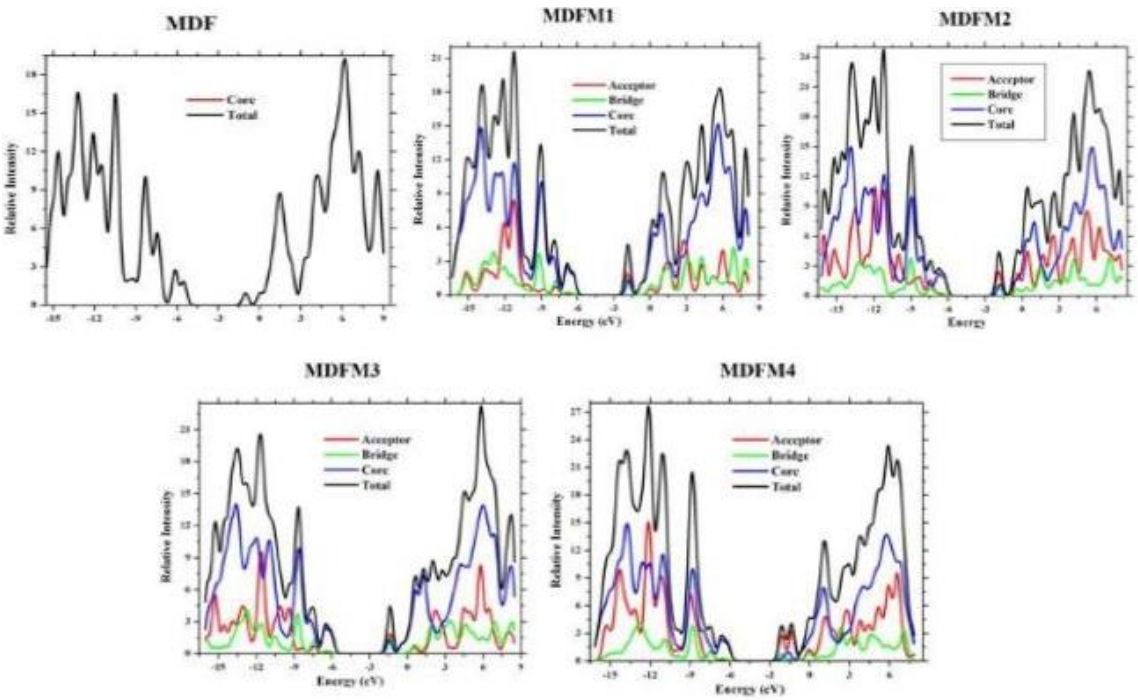

Figure 4. DOS for representative MDF and developed compound MDFM1-MDFM4 at CAM-B3LYP as well as 6-31G (d, p) basis sets.

The electron charge density in the HOMO of MDFM1 and MDFM2 is mainly on the core, with some on the acceptor and bridge. The LUMO has a similar distribution. MDFM3's HUMO has most of the charge density on the core, with some on the bridge and acceptor. MDFM4's HOMO has significant contributions from the core and acceptor in the charge density, with less from the bridge. The LUMO has a similar pattern.

3.5. Molecular Electrostatic Potential Analysis

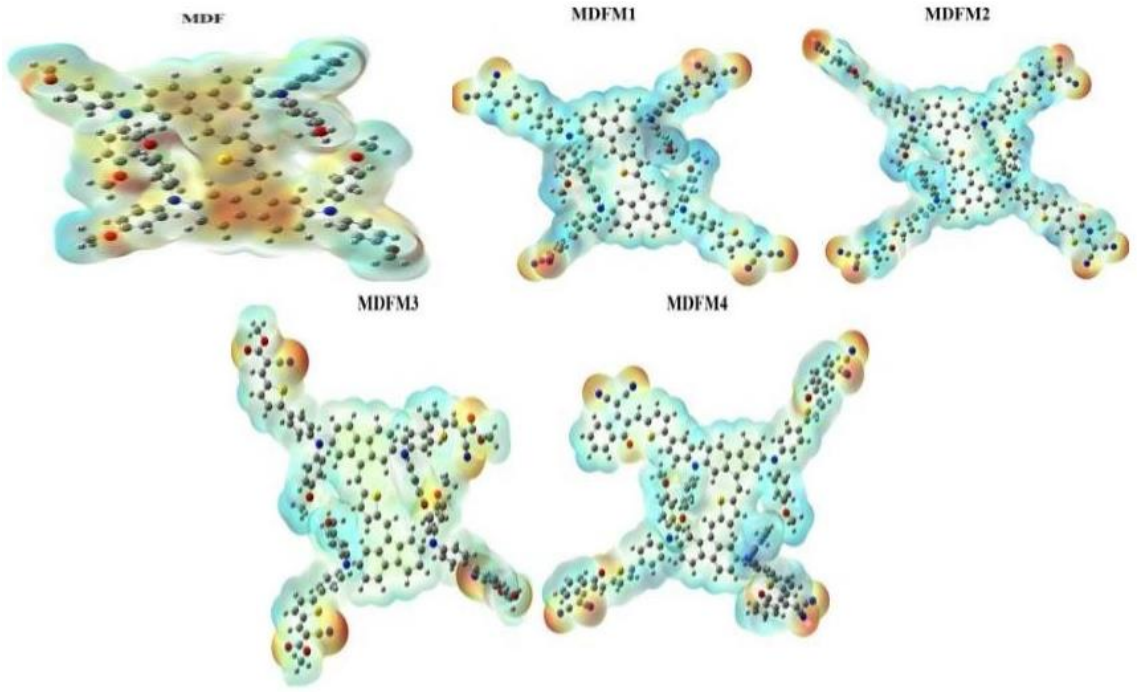

Figure 5. Analysis of the (MDFM1-MDFM4) designed molecules' molecular electrostatic potential and the reference MDF.

MEP determines the majority as well as the deficiency of electron density of all design molecules (MDFM1 to MDFM4) with the reference MDF (Figure 5). In MEP maps, there are three colors (blue, green, and red) displays which shown the different properties of the molecule. The blue color indicates a negative charge-deficient (not enough positive charges) area, while the red color reveals the electron-rich (negative charges), and green indicates the electrically neutral area.

It was interestingly discovered that all the design molecules (MDFM1-MDFM4) had the same division pattern, while the reference molecules had a unique pattern, demonstrating how well the designed molecules were created for solar cell applications. All developed molecules' end cap acceptors have negative charges (red color), whereas reference end caps have positive charges. Designed molecules' separate donor units each contain positive charges, while the middle component is neutral (green color). However, the center of the molecule is dominated by the color red. Figure 5 indicates that the acceptor of the newly developed compound MDFM4 has more lone pairs than the other designed molecule; it has a more negative charge distribution, whereas the end of the reference molecule MDF has smaller blue patterns.

3.6. Optical Properties

The developed compounds' (MDFM1-MDFM4) estimated optical characteristics at TD-CAM- B3LYP with basis set 6-31G (d, p), and their findings are mentioned in Tables 2-3. For the purpose of developing effective photovoltaic materials, the quality is dependent on the molecule's broad and strong absorption properties. To investigate the photo-physical properties of the reference molecule, we performed optimization calculations in both gas and solvent states. Using various methods like B3LYP, CAM-B3LYP, MPW1PW91, and ωB97XD under TD-SCF as well as 6-31G (d, p) models. The UV values derived from TD-CAM-B3LYP/6-31G (d, p) for the representative molecule are highly consistent with experimental outcomes. The theoretical study shows that the spectral absorption (computed λmax) of the representative molecule MDF in the THF is 424.06 nanometers. Therefore, this methodology is used for examining the photo-physical characteristics of all created molecules. For each designing molecule with the reference MDF, six electronic transition states of the designing molecules and 10 of the reference molecules are noted in both the gas and solution phase. The noted wave length (λmax), experimental wave length (λmax), excited energies (Ex), oscillating strength (f), dipole moments (D), and % e- transporting contributions (%ETCs) for representative compound and others design compound at TD-CAM-B3LYP as well as basis sets 6-31G (d, p) gaseous state value displayed in Table 2 and Table 3 for the solvents state and their photovoltaic performance in the tables.

Table 3. *Values were calculated for all design molecules and reference MDF comp. λmax, experiment value λmax, Dipole moments (D), % electrons transporting contribution (%ETCs) of representative MDF and designed molecules.*

Molecules	Cal λmax (Nanometer)	Experiment λmax (Nanometers)	F (au)	%ETCs	Ex (electron Volts)	Dipole Moment
MDF	416.44	455	0.9766	H → L+1 (61%)	2.9772	3.2088
MDFM1	409.52	455	2.3704	H → L+1 (46%)	2.9221	15.0960
MDFM2	437.44	455	3.5230	H → L+1 (35%)	2.8343	8.0700
MDFM3	400.07	455	1.7888	H → L+1 (56%)	2.9124	6.8038
MDFM4	460.93	455	2.4876	H → L+1 (40%)	2.6899	7.6824

Table 4. *Values calculated for all design molecules and representative MDF cal. λ**max**, experiment value λmax, Dipole moments (D), % electrons transported contributions (%ETCs) of representative MDF and developed compounds in THF solvent.*

Molecules	Cal λmax (nanometer)	Experiment λmax (nanometers)	F (au)	%ETCs	Ex (electron Volts)	Dipole moments
MDF	424.06	455	1.1785	H → L+1 (65%)	2.9237	4.2333
MDFM1	439.27	455	2.8395	H → L+1 (37%)	2.8225	18.1745
MDFM2	449.62	455	3.6363	H → L+1 (29%)	2.7340	9.7645
MDFM3	434.43	455	2.1955	H → L+1 (38%)	2.8540	9.2640
MDFM4	485.83	455	2.4791	H → L+1 (33%)	2.5520	9.4766

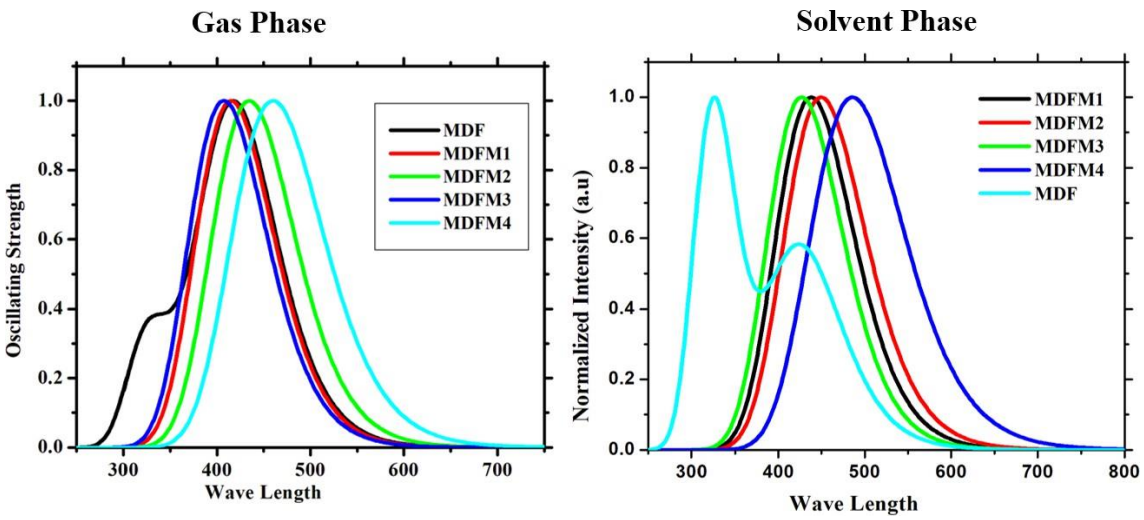

Figure 6. *Shows the absorption pattern lines of all design compounds, as well as the reference MDF, and TD-CAM-B3LYP/6-31G. (d, p).*

3.7. Reorganization Energy

Reorganization energy is important for assessing organic solar cell progress and electron/hole behavior. The degree of reorganization is inversely correlated with the charge transfer, and as such, low levels of reorganization are associated with high charge mobility resulting from energy. The reorganization energy of holes and electrons is determined by using Equations (1) and (2). Charge transfer is evaluated through internal (λint.) and external (λext.) reorganizational energy [29]. The evaluation of internal geometrical changes was conducted through the measurement of inner reorganization energy. Specifically, the internal reorganization energy was utilized as a quantitative indicator of internal structural changes [30]. Our research excluded consideration of external energy changes, as they were deemed irrelevant to our investigation. Thus, the focus was solely on internal reorganization energy. Table 4 displays the values of both internal and external reorganization energies for all molecules examined in our study.

Table 5. *Reorganizational energy of MDF and all design compounds.*

Molecule	λ e (e Volts)	λ h (e Volts)
MDF	0.0307	0.0177
MDFM1	0.0315	0.0201
MDFM2	0.0257	0.0250
MDFM3	0.0213	0.0232
MDFM4	0.0144	0.0250

It has been determined that the MDF molecule has a λe finding of 0.0307 eV. However, when contrasted to the other designed molecules, all of them have lower values except for MDFM1. The compound MDFM4 has a minimum reorganization energy of electrons, revealing that the donor and acceptor parts have the maximum charge motilities. The electron reorganization energy of all the compounds follows a decreasing order of MDFM1>MDF>MDFM2>MDFM3>MDFM4. The λh value of MDF has been computed to be 0.2405 eV, which is less than the reference value for all the developed molecules except for MDFM2 and MDFM4, which have the same value. Among all the developed molecules, MDFM1 has the least value and is found to be the best molecule for hole-transporting motilities, even better than the reference molecule MDF.

Further discussion results that MDFM2 and MDFM4 are best for current transport motilities, and MDFM1 is best for the hole transferred. On the contrary, as compared to a synthetic reference molecule, MDFM3 has a higher electron and hole reorganizational energy value. Hence, it might be utilized as a useful donor material for solar cell applications.

3.8. Di-polarities

The di-polarities of organic solar cells are recognized as a crucial performance indicator [31]. This is due to the fact that the solubility of these cells is linked to the dipolarities of the material; a greater dipolarity value results in higher solubility capacity in organic solvents [32]. Solubility tends to be higher in OSCs that have a higher proportion of polar atoms. According to the reference (MDF), the di-polarity in both the gaseous phase and solvent phase is estimated to be low [33]. The values of di-polarity for the design molecules MDFM1 to MDFM4 and the reference MDF in the solvent THF were analyzed using the CAM-B3LYP/6-31G (d, p) method, and the outcomes are displayed in Table 5. Interestingly, the di-polarity of the design molecules MDFM1 to MDFM4 is highest in the solvent states than in the gas states. In the solvent phase, the order of the dipolarity moment is MDFM1>MDFM2>MDFM4>MDFM3>MDF, and this order

is the same in the gas state as well.

Table 6. Dipole moments in excites state, ground states, and the distinction between them for MDF and MDFM1-MDFM4.

Molecule	μg	μe	μe - μg
MDF	3.2088	4.2333	1.0245
MDFM1	15.0960	18.1745	3.0785
MDFM2	8.0699	9.7645	1.6946
MDFM3	6.8038	9.2640	2.4602
MDFM4	7.6824	9.4766	1.7942

The dipole moments of all the molecules that have been developed were examined, and they were found to be higher than the reference in both the gases and solvent phases. This increased dipole moment leads to the self-organization of the design molecules, forming extensive chains that facilitate a robust pathway for charge transfer.

Open circuit voltage (VOC)

VOC is measured by the highest potential outcomes that can be obtained from OSCs [34]. It indicates the highest quantity of voltages that the cell can generate when it is not connected to any external circuit [35]. The voltage levels of the accepting and donating molecules that make up the solar cell's EHOMO and ELUMO closely correlate with the magnitude of VOC. Theoretical values of VOC can be calculated using a specific equation.

$$V_{OC} = (|E^D| - |E^A|) - 0.3 \quad (3)$$

HOMO - LUMO

The HOMO-LUMO energy gaps for MDF, MDFM1 to MDFM4 are 4.44 V, 4.41 V, 4.30 V, 4.52 V, and 4.00 V, respectively (HOMO donor - LUMO acceptor). All of the analyzed molecules' VOC values are in the following order: MDF>MDFM3>MDFM4> MDFM2>MDFM1. The VOC calculations rely on the accepting molecule and the donating molecule, as previously discussed. Low LUMO values in the acceptor lead to greater VOC values and improved optoelectronic characteristics. Moreover, it is becoming more common for donor molecules to shift electrons from their HOMO states to directly achieve optoelectronic characteristics. Moreover, the PEC values are obtained from the E_{HOMO}-L_{UMO} gaps of the acceptor and donor.

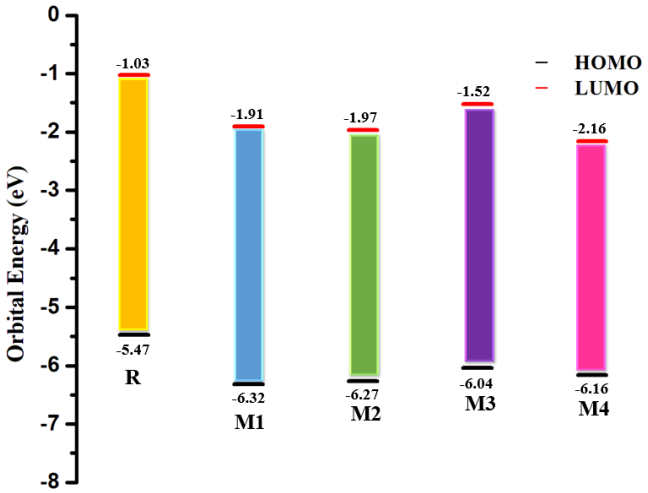

Figure 7. The proposed Donors MDFM1–MDFM4 molecular orbital energy diagram comprised the reference (MDF).

Figure 7 provides evidence that in the analyzed molecules (MDF, MDFM1 to MDFM4), the donor's LUMO level is higher than the acceptor's LUMO level. It facilitates charge density transfer from the examined molecule's donor to its acceptor, displaying the optoelectronic capabilities of all investigated compounds in more effective methods.

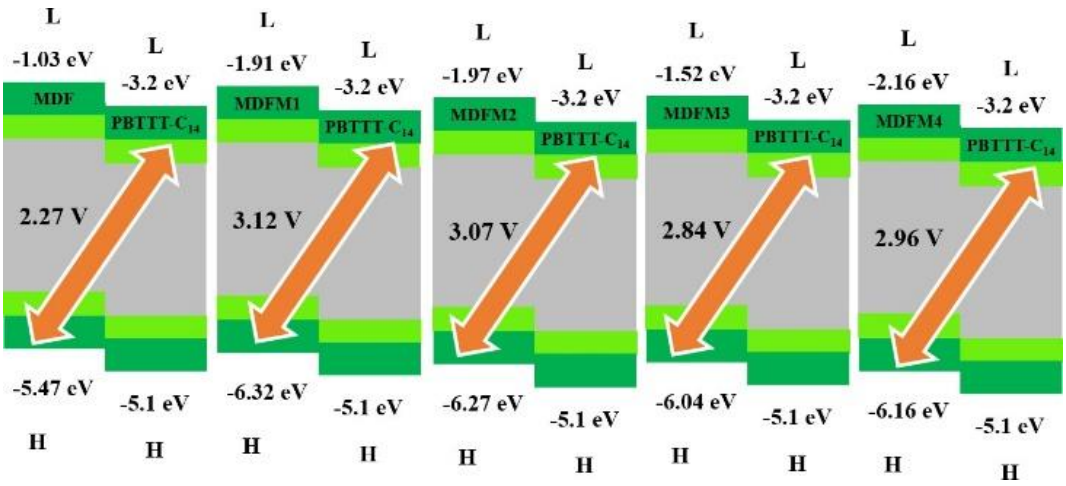

Figure 8. Open Circuit voltage values of Reference MDF and Design Molecules MDFM1 to MDFM4 compared with the corresponding acceptor material PBTTT-C14.

3.9. Transition Density Matrix and Excited Binding Energies

The transitional density of the matrix (TDMs) is supposed to be a precious technique for studying and illustrating electronic transition processes in OSCs [36]. By providing a unique three- dimensional map, TDMs enable one to determine the coherence lengths and delocalization for each electronic TDM between two intrinsic states of the developed molecule [37]. TDMs are utilized to explain charge-movement excitations in OSCs [38]. The emission and absorption of the design molecules MDFM1-MDFM4 and base compound MDF are analyzed up to six excited states by utilizing the CAM-B3LYP/6-31G (d, p) models. This analysis is conducted using the Multiwfn 3.8 software CAM-B3LYP/6-31G (d, p) /TD (n states=6) hybrid model. The role of hydrogen has been overlooked due to its minor contribution to the electronic transition. To study the electronic charge density of molecules at the CAM-B3LYP by using basis sets 6- 31G (d, p), we segmented the molecules into various components, such as cores, acceptors, and bridge components. Figure 8 illustrates the segmentation of these molecules into different segments (indicated by atoms numbered sequentially from 1 to the total number of atoms in the molecule) at the bottom, while the electron density is displayed on the y-axis on the left side.

Our TDM studies indicate that charge coherence is prevalent in all compounds. Charge coherence is observed on the donor side of reference compounds. Moreover, charge coherence can be observed in donors and bridging units in MDFM1. Interestingly, MDFM2-MDFM4 molecules appear to be more coherent than MDFM1. Our analysis of electron coherence behavior in developed molecules MDFM1-MDFM4 and reference (MDF) reveals that current coherence transfers from the donor to the bridging block. This bridging block facilitates electron transport without trapping them, and the current density is eventually transferred to the acceptor molecule.

Our findings suggest that electron coupling in all investigated compounds may be less than that of the reference, but exciton dissociation in the excited state could be greater and simpler. Binding energy is a useful method for evaluating the performance of organic solar cells. This approach involves calculating the Coulombic interaction between the electrons and holes in the system [39]. Compounds with low binding energy exhibit weak Coulombic interactions between electrons and holes, and the opposite holds for those with high binding energy. The binding energy value is defined as the difference between the band gap and the minimum excitation energy required for the first electron-hole excitation [40]. This technique offers a valuable tool for assessing the progress of photovoltaic cells in scientific research [41]. Equation (4) may be used to compute binding energy.

$$E_b = E_{H\text{-}L} - E_{opt} \quad (4)$$

Table 7. *Displays the values of all molecules' binding energy under consideration. It is observed.*

Molecules	EHOMO-LUMO (eV)	Eopt (eV)	Eb (eV)
MDF	4.4400	2.9772	1.4628
MDFM1	4.4100	2.9221	1.4879
MDFM2	4.3000	2.8343	1.4657
MDFM3	4.5200	2.9124	1.6076
MDFM4	4.0000	2.6899	1.3101

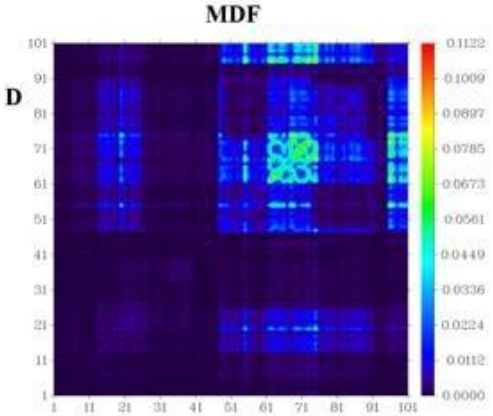

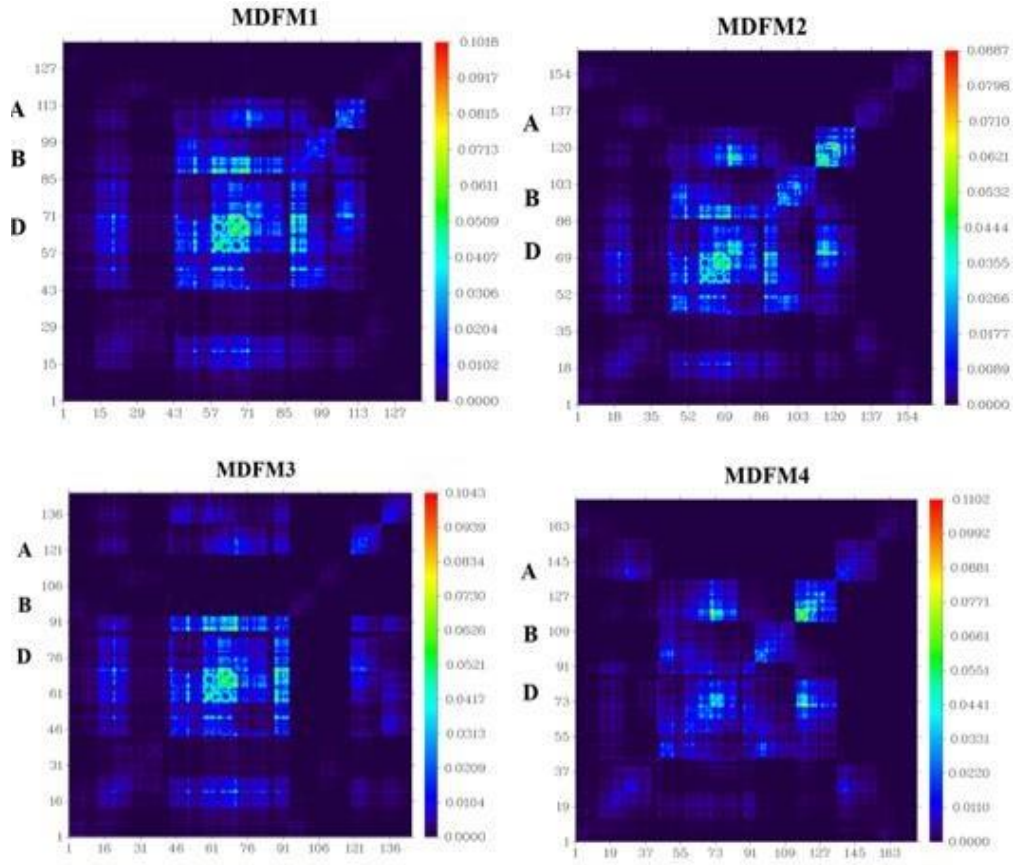

Figure 9. *Diagram of TDM values of Reference molecule MDF and all design molecules MDFM1 to MDFM4.*

Table 5 evaluated the HOMO-LUMO band gap**,** first singlet excitation energy (Eopt), and exciton binding energy (Eb). The MDFM4 molecule exhibits a lower binding energy value, resulting in its facile dissociation into separated charges. Conversely, the MDFM3 molecule possesses a higher binding energy, making it less prone to dissociation. In comparison to the reference molecule MDF, all the newly developed compounds exhibit minimum exciton binding energy (Eb), consequently leading to maximum current dissociation progress. The binding energy values of all studied molecules, in increasing order, are *MDFM4* < *MDF* < *MDFM2* < *MDFM1* < *MDFM3*. Additionally, the results of all the design molecules and the base molecule MDF for the TDM demonstrate good agreement.

4. Conclusion

Four novel organic molecules, MDFM1-MDFM4, were rationally designed as donor materials for high-efficiency organic solar cells. Their optoelectronic properties were systematically investigated using Density Functional Theory with four different functionals: B3LYP, CAM-B3LYP, MPW1PW91, and ωB97XD, all paired with the 6-31G (d, p) basis set. Among the tested methods, CAM-B3LYP/6-31G (d, p) proved to be the most reliable, as it yielded values for the reference molecule MDF that showed the closest agreement with experimental data. Therefore, this level of theory was selected for all subsequent calculations on MDFM1-MDFM4. A detailed comparative study was performed between the designed molecules and the parent MDF molecule, focusing on: HOMO-LUMO energy levels, bandgap energy, and frontier molecular orbital distribution. All four designed molecules MDFM1-MDFM4 exhibited significantly reduced HOMO-LUMO gaps compared to MDF, indicating improved intramolecular charge transfer character. UV/vis absorption spectra were simulated via TD-DFT. The designed molecules showed strong bathochromic shifts with absorption maxima extended into the visible and near-IR region. This red-shifted, broadened absorption enhances sunlight harvesting capability. Dipole moments, reorganization energies, and charge mobility for both electrons and holes were evaluated. MDFM1-MDFM4 demonstrated higher dipole moments and lower reorganization energies than MDF, suggesting superior charge separation and more balanced electron/hole transport molecules. Exciton binding energies, open-circuit voltage (VOC), fill factor, and light-harvesting efficiency were estimated. The designed compounds exhibited lower exciton binding energies and higher predicted VOC values, both critical for improved power conversion efficiency. The computational results clearly demonstrate that MDFM1-MDFM4 outperform the reference MDF molecule in all key photovoltaic metrics. The

synergistic combination of narrower band gaps, enhanced absorption coefficients, efficient charge transport, and favorable photovoltaic parameters makes these newly designed molecules highly promising candidates for next-generation organic solar cells. Based on these DFT findings, MDFM1-MDFM4 are strongly recommended for experimental synthesis and fabrication into OSC devices. They hold significant potential to boost the performance of organic photovoltaic technologies.

Abbreviations

OSCs	Organic Solar Cells
PCE	Power Conversion Efficiency
DFT	Density Functional Theory
TD-DFT	Time-Dependent Density Functional Theory
HTMs	Hole-Transporting Materials
OPVs	Organic Photovoltaics
EA	Electron Affinity
IP	Ionization Potentials
MO	Molecular Orbitals
IEFPCM	Integrated Equation Formalism Polarizable Continuum Model
TDM	Transition Density Matrix
FMOs	Frontier Molecular Orbitals
EDOS	Electronic Density Of STATE
MEP	Molecular Electrostatic Potential
TDMs	Transitional Density Of The Matrix

Acknowledgments

This research article was written by the author and co-authors without any external financial support. The draft of this work, including writing, graphics, and design, was carried out at the Department of Chemistry, University of Agriculture, Faisalabad (38000), Punjab, Pakistan.

Author Contributions

Abaid Ullah: Conceptualization, Formal Analysis, Investigation, Supervision

Usman Ibrahim: Data curation, Formal Analysis, Investigation, Validation, Writing – review & editing

Samina Liaqat: Investigation, Writing – review & editing

Muhammad Javid: Formal Analysis, Funding acquisition, Validation

Wajiha Shehbaz: Supervision, Writing – original draft, Writing – review & editing

Rimsha Shareef: Validation, Writing – original draft

Sabahat Asghar: Formal Analysis, Investigation, Validation, Writing – original draft

Muhammad Sajid Abbas: Conceptualization, Investigation, Writing – review & editing

Muhammad Hasnain: Conceptualization, Funding acquisition, Investigation, Project administration

Conflicts of Interest

The authors declare no conflicts of interest.

References

[1] Kallio, S. M., & Mäenpää, J. (2025). Visuality as an affordance on Instagram news production. *Digital Journalism*, 1-19. https://doi.org/10.1080/21670811.2025.2462558

[2] Bhuiyan, M. R. A. (2022). Overcome the future environmental challenges through sustainable and renewable energy resources. *Micro & Nano Letters*, *17*(14), 402-416. https://doi.org/10.1049/mna2.12148

[3] Franjić, S. (2023). Unleashing sustainable energy: the sun, Earth's largest and most powerful source. *Journal of Sustainable Development*, *4*(2), 1-9. https://doi.org/10.56388/susd

[4] Lv, J., Xie, J., Mohamed, A. G. A., Zhang, X., Feng, Y., Jiao, L.,... & Wang, Y. (2023). Solar utilization beyond photosynthesis. *Nature Reviews Chemistry*, *7*(2), 91-105. https://doi.org/10.1038/s41570-022-00448-9

[5] Rathore, N., Panwar, N. L., Yettou, F., & Gama, A. (2021). A comprehensive review of different types of solar photovoltaic cells and their applications. *International Journal of Ambient Energy*, *42*(10), 1200-1217. https://doi.org/10.1080/01430750.2019.1592774

[6] Kant, N., & Singh, P. (2022). Review of next-generation photovoltaic solar cell technology and comparative materialistic development. *Materials Today: Proceedings*, *56*, 3460-3470. https://doi.org/10.1016/j.matpr.2021.11.116

[7] Ballif, C., Haug, F. J., Boccard, M., Verlinden, P. J., & Hahn, G. (2022). Status and perspectives of crystalline silicon photovoltaics in research and industry. *Nature Reviews Materials*, *7*(8), 597-616. https://doi.org/10.1038/s41578-022-00423-2

[8] Shah, N., Shah, A. A., Leung, P. K., Khan, S., Sun, K., Zhu, X., & Liao, Q. (2023). A review of third-generation solar cells. *Processes*, *11*(6), 1852. https://doi.org/10.3390/pr11061852

[9] Yu, H., Wang, J., Zhou, Q., Qin, J., Wang, Y., Lu, X., & Cheng, P. (2023). Semi-transparent organic photovoltaics. *Chemical Society Reviews*, *52*(13), 4132-4148. https://doi.org/10.1039/d3cs00233k

[10] Wan, X., Li, C., Zhang, M., & Chen, Y. (2020). Acceptor–donor–acceptor type molecules for high-performance organic photovoltaics–chemistry and mechanism. *Chemical Society Reviews*, *49*(9), 2828-2842. https://doi.org/10.1039/d0cs00084a

[11] Wang, X., Sun, Q., Gao, J., Wang, J., Xu, C., Ma, X., & Zhang, F. (2021). Recent progress of organic photovoltaics with efficiency over 17%. *Energies*, *14*(14), 4200. https://doi.org/10.3390/en14144200

[12] Tracey, F. M. (2024). *Synthesis of organic materials for optoelectronic applications* (Doctoral dissertation, University of Glasgow). https://theses.gla.ac.uk/84295/

[13] Kim, I. B., Jang, S. Y., Kim, Y. A., Kang, R., Kim, I. S., Ko, D. K., & Kim, D. Y. (2017). The effect of fluorine substitution on the molecular interactions and performance in polymer solar cells. *ACS applied materials & interfaces*, *9*(28), 24011-24019. https://doi.org/10.1021/acsami.7b04214

[14] Yang, X., Shao, Y., Wang, S., Chen, M., Xiao, B., Sun, R., & Min, J. (2025). Processability considerations for next-generation organic photovoltaic materials. *Advanced Materials*, *37*(31), 2307863. https://doi.org/10.1002/adma.202307863

[15] Harito, C., Khalil, M., Nurdiwijayanto, L., Septiani, N. L. W., Abrori, S. A., Putra, B. R.,... & Walsh, F. C. (2024). Facet-controlled growth and soft-chemical exfoliation of two-dimensional titanium dioxide nanosheets. *Nanoscale Advances*, *6*(17), 4325-4345. https://doi.org/10.1039/d4na00442f

[16] Majeed, M., Waqas, M., Aloui, Z., Essid, M., Ibrahim, M. A., Khera, R. A.,... & Ans, M. (2023). Exploring the electronic, optical, and charge transfer properties of ADA-type IDTV-ThIC-based molecules to enhance the photovoltaic performance of organic solar cells. *ACS omega*, *8*(48), 45384-45404. https://doi.org/10.1021/acsomega.3c04437

[17] Yakalı, G. (2021). Examination of aggregation-induced enhanced emission in a propeller-shaped chiral nonconjugated blue emitter from restricted intramolecular rotation and J-type π··· π stacking interactions. *Physical Chemistry Chemical Physics*, *23*(19), 11388-11399. https://doi.org/10.1039/d0cp06690g

[18] Akram, W., Zahid, W. A., Peng, T., Al-Shagri, L. M., Wang, K., & Iqbal, J. (2024). Terminal Acceptor-Driven designing of fused Triphenylamine-Based organic small molecules with Bis-Dimethylfluorenyl peripheral moieties for advanced photovoltaics. *Solar Energy*, *277*, 112749. https://doi.org/10.1016/j.solener.2024.112749

[19] Zhou, B., Dai, T., Zhou, J., Chen, Y., Geng, Y., Lei, P.,... & Zhou, E. (2024). Conjugated D–π–A photovoltaic polymers containing thieno [3, 2-b] thiophene π-bridge. *Materials Chemistry Frontiers*, *8*(6), 1563-1590. https://doi.org/10.1039/d3qm00849e

[20] Murugan, P., Hu, T., Hu, X., & Chen, Y. (2022). Advancements in organic small molecule hole-transporting materials for perovskite solar cells: past and future. *Journal of Materials Chemistry A*, *10*(10), 5044-5081. https://doi.org/10.1039/d1ta11039j

[21] Elmorsy, M. R., Badawy, S. A., Alnakeeb, A., Fadda, A. A., Ismail, M. A., & El Salam, M. A. (2025). Insecticidal evaluation of new cyanoacetamide derivatives against Spodoptera littoralis: molecular docking and density function theory approaches. *Journal of Agricultural and Food Chemistry*, *73*(18), 10751-10763. https://pubs.acs.org/doi/10.1021/acs.jafc.4c12449

[22] Mushtaq, Z., Ahad, A., Asghar, S., Abbas, M. S., Zafar, A., Majeed, A.,... & Ejaz, S. (2026). Optimizing π-conjugated systems of spiro-based HTMs: structures and concept towards boosting efficiency of PSCs. *Sustainable Energy & Fuels*, *10*(1), 137-149. https://doi.org/10.1039/d5se01025j

[23] Zafar, W., Noreen, S., Elnaggar, A. Y., Mahmoud, M. H., & Azab, I. H. E. (2025). Experimental and theoretical studies on a new urea clathrate crystal: X-ray diffraction, Hirshfeld surface analysis, RDG− NCI, FMOs, and NBO analysis. *Brazilian Journal of Physics*, *55*(3), 125. https://doi.org/10.1007/s13538-025-01753-6

[24] Fuse, M., Mazzeo, G., Ghidinelli, S., Evidente, A., Abbate, S., & Longhi, G. (2024). Experimental and theoretical aspects of magnetic circular dichroism and magnetic circularly polarized luminescence in the UV, visible, and IR ranges: A review. *Spectrochimica Acta Part A: Molecular and Biomolecular Spectroscopy*, *319*, 124583. https://doi.org/10.1016/j.saa.2024.124583

[25] Naz, H., Adnan, M., Irshad, Z., Hussain, R., Darwish, H. W., & Ahmed, M. (2024). Elucidating the advancement in the optoelectronics characteristics of benzoselenadiazole-based A2-D-A1-D-A2-type nonfullerene acceptors for efficient organic solar cells. *ACS omega*, *9*(44), 44668-44688. https://doi.org/10.1021/acsomega.4c07436

[26] Hu, H., Zhang, R., Jiang, D., Mu, X., Yi, J., Yu, H.,... & Yin, H. (2025). Revealing electron transport connectivity as an important factor influencing the stability of organic solar cells. *Nature Communications*, *16*(1), 6546. https://doi.org/10.1038/s41467-025-60599-3

[27] Hussein, H. A., & Fadhil, G. F. (2023). Theoretical investigation of para-aminodichloro chalcone isomers. Part II: a DFT structure–stability study of the FMO and NLO properties. *ACS omega*, *8*(5), 4937-4953. https://doi.org/10.1021/acsomega.2c07148

[28] Dhifaoui, S., Azaid, A., Bourass, M., Ben Haj Hassen, L., Nasri, H., & Bouachrine, M. (2021). DFT studies on molecular Structure, absorption properties, NBO analysis, and Hirshfeld surface analysis of Iron (III) porphyrin complex. *Physical Chemistry Research*, *9*(4), 701-713. https://doi.org/10.22036/pcr.2021.272919.1886

[29] Hussain, M., Naz, H., Irshad, Z., Hussain, R., Darwish, H. W., Ahmed, M.,... & Adnan, M. (2026). Molecularly modified quinoxaline-based unfused nonfullerene acceptors for efficient and stable organic photovoltaics. *Journal of Computational Biophysics and Chemistry*, *25*(11), 2469-2492. https://doi.org/10.1142/S2737416526500183

[30] Kose, M. E., & Schanze, K. S. (2020). Prediction of internal reorganization energy in photoinduced electron transfer processes of molecular dyads. *The Journal of Physical Chemistry A*, *124*(45), 9478-9486. https://pubs.acs.org/doi/10.1021/acs.jpca.0c09533

[31] Srinath, Patil, O., Devar, S., & Hanagodimath, S. M. (2025). Estimation of Electric Dipole Moment by Solvatochromism, Computational Method, and Study of the Effect of Solvents by Preferential Solvation of 6–Methoxy—4—(4—Nitro—Phenoxy Methyl)—Chromen—2—One (6mnpm). *Journal of Fluorescence*, *35*(7), 5861-5869. https://doi.org/10.1007/s10895-024-03955-8

[32] Srinath, Chillargikar, S., Patil, O., & Hanagodimath, S. M. (2025). Experimental and theoretical approach to estimate electric dipole moments and analysis of Preferential solvation, fluorescence quenching of 4-NPMB coumarin molecule by the steady state method. *Journal of Fluorescence*, *35*(11), 10821-10831. https://doi.org/10.1007/s10895-025-04331-w

[33] Bagewadi, B. I., Ingalagondi, P. K., & Gounhalli, S. G. (2026). DFT and TD-DFT Insights into the Solvatochromic and Electronic Properties of a Quinoline Derivative (E1QPH). *Journal of Fluorescence*, *36*(5), 3343-3351. https://doi.org/10.1007/s10895-026-04769-6

[34] Wang, J., Xu, H., Xiao, Y., Li, T., Wang, J., Liu, K.,... & Chen, X. (2020). A thiophene-fused benzotriazole unit as a "π-bridge" in A-π-D-π-A type acceptor to achieve more balanced JSC and VOC for OSCs. *Organic Electronics*, *82*, 105705. https://doi.org/10.1016/j.orgel.2020.105705

[35] An, N., Cai, Y., Wu, H., Tang, A., Zhang, K., Hao, X.,... & Zhou, E. (2020). Solution-processed organic solar cells with a high open-circuit voltage of 1.3 V and low non-radiative voltage loss of 0.16 V. *Advanced Materials*, *32*(39), 2002122. https://doi.org/10.1002/adma.202002122

[36] Salwa, Adnan, M., Irshad, Z., Hussain, R., Darwish, H. W., Hussain, F., & Ahmed, M. (2025). Improving Optoelectronic Properties of Acceptor–Donor–Acceptor-Type Non-Fullerene Acceptors Containing Extended Fused Ring Donor Units for Efficient Organic Semiconductors. *Energy Technology*, *13*(3), 2401529. https://doi.org/10.1002/ente.202401529

[37] Hussain, M., Adnan, M., Irshad, Z., Hussain, R., Darwish, H. W., & Lim, J. (2024). Correlating chemical structure and charge carrier dynamics in phenanthrocarbazole-based hole transporting materials for efficient perovskite solar cells. *Journal of Physical Organic Chemistry*, *37*(12), e4662. https://doi.org/10.1002/poc.4662

[38] Sadiq, S., Khera, R. A., Tawfeek, A. M., Ibrahim, M. A., Abbas, F., Ali, S.,... & Waqas, M. (2024). Theoretical investigation of substituted end groups in thiophene-phenyl-thiophene (TPT) derivatives for high-efficiency organic solar cells. *Journal of Physical Organic Chemistry*, *37*(6), e4607. https://doi.org/10.1002/poc.4607

[39] Fu, J., Ramesh, S., Melvin Lim, J. W., & Sum, T. C. (2023). Carriers, quasi-particles, and collective excitations in halide perovskites. *Chemical reviews*, *123*(13), 8154-8231. https://doi.org/10.1021/acs.chemrev.2c00843

[40] Kashani, S., Rech, J. J., Liu, T., Baustert, K., Ghaffari, A., Angunawela, I.,... & Ade, H. (2024). Exciton binding energy in organic polymers: experimental considerations and tuning prospects. *Advanced Energy Materials*, *14*(6), 2302837. https://doi.org/10.1002/aenm.202302837

[41] Niedzwiedzki, D. M., Zhou, H., & Biswas, P. (2022). Exciton binding energy of MAPbI3 thin film elucidated via analysis and modeling of perovskite absorption and photoluminescence properties using various methodologies. *The Journal of Physical Chemistry C*, *126*(2), 1046-1054. https://pubs.acs.org/doi/10.1021/acs.jpcc.1c09598